Biomaterials Science

ROYAL SOCIETY OF CHEMISTRY

PAPER

View Article Online
View Journal | View Issue

Cite this: *Biomater. Sci.*, 2024, **12**, 3163

Platelet membrane encapsulated curcumin nanomaterial-mediated specific thrombolysis and anti-thrombotic treatment among pregnant women

Lin Xu,†[a,c,e,f] Yijie Zhou,†[a,c,e,f] Na Li,†[a,c,e] Anyu Yang *[e] and Hongbo Qi*[b,c,d]

Received 27th January 2024,
Accepted 15th April 2024

DOI: 10.1039/d4bm00149d

rsc.li/biomaterials-science

The current treatment for venous thrombosis during pregnancy is ineffective, primarily, due to the unique physiology of pregnant women. Most clinical medications have fetal side effects when they circulate in the body. We first synthesized nanomaterials (Cur–PFP@PC) using poly lactic-co-glycolic acid (PLGA) as the base material, with curcumin (Cur) and perfluoropentane (PFP) as core components. Subsequently, we encapsulated Cur–PFP@PC into the platelet membrane to synthesize P-Cur–PFP@PC. Under ultrasound guidance, in combination with low-intensity focused ultrasound (LIFU), PFP underwent a phase change, resulting in thrombolysis. The generated microbubbles enhanced the signal impact of ultrasound, and P-Cur–PFP@PC showed better performance than Cur–PFP@PC. P-Cur–PFP@PC can target thrombosis treatment, achieve visually and precisely controlled drug release, and repair damaged blood vessels, thus avoiding the adverse effects associated with traditional long-term drug administration.

1. Introduction

Venous thromboembolism (VTE) is the third most common cardiovascular disease, encompassing deep vein thrombosis (DVT) and pulmonary embolism (PE) and ranges 1–2‰ annually in the general population.[1–3] With existing treatment methods, recurrence rates and complications remain high.[4] The adhesion of platelets to an injured vessel wall and platelet activation are critical events in the formation of a thrombus.[5] Pregnancy is a significant high-risk factor for VTE, with a 5-fold higher risk.[6] VTE is one of the major cardiovascular causes of morbidity and mortality in pregnant women. Pregnancy-related venous thrombosis can result in miscarriages, fetal intrauterine growth restriction, gestational hypertension, and placental abruption, posing a severe threat to the lives of both the mother and the child. Furthermore, the quality of life in the diagnosed patients is diminished by post-thrombotic syndrome.[1–3,7,8] Clinically, most thrombolytic drugs have short half-lives, necessitating repeated administration within a short period, thereby adding additional risks to the treatment. Heparin is primarily used for the prevention and treatment of pregnancy-related venous thrombosis. However, prolonged use of heparin can lead to miscarriages, osteoporosis, congenital malformations in fetuses, bleeding, and neurodevelopmental disorders. Thus, heparin treatment can introduce additional risks.[9] Moreover, it weakens the physiological protective state of pregnancy (hypercoagulable state), leading to severe bleeding such as cerebral hemorrhage.[10]

Biomimetic technology has achieved significant success across various fields. Recently, natural cell membranes have been widely applied in different cell types.[11] In this kind of design, a nanomaterial is covered by a natural cell membrane layer, which constitutes a primary structural component of cells and extracellular vesicles, mimicking the surface functionality of natural cells.[12] This enables the nanomaterial to directly mimic the characteristics of source cells, improving site-specific accumulation and efficacy, thus eliminating the need for complicated chemical synthesis modification and processing. This kind of material often exhibits remarkable biocompatibility and stealthiness,[13–15] even emulating physical properties, including morphology and flexibility.[16] Currently, this nanobiomimetic technology has made substantial progress in fundamental research related to cancer and cardiovascular and cerebrovascular disease diagnosis and treatment.[17–19] However, its usefulness in the field of preg-

[a]*The Department of Obstetrics, The First Affiliated Hospital of Chongqing Medical University, Chongqing 400016, China*
[b]*Women and Children's Hospital of Chongqing Medical University, Chongqing 401147, China. E-mail: qihongbocy@gmail.com*
[c]*Chongqing Key Laboratory of Maternal and Fetal Medicine, Chongqing Medical University, Chongqing 400016, China*
[d]*Joint International Research Laboratory of Reproduction and Development of Chinese Ministry of Education, Chongqing Medical University, Chongqing 400016, China*
[e]*Institute of Ultrasound Imaging, the Second Affiliated Hospital of Chongqing Medical University, Chongqing 400010, China*
[f]*Guiyang Maternal and Child Health Care Hospital, Guiyang 550002, Guizhou, China*
†These authors contributed equally to this work and can be considered as co-first authors.

nancy-related venous thrombosis remains unexplored. Presently, targeted treatment for pregnancy-related venous thrombosis faces two significant challenges: safety and targeting. The drug components used by pregnant women during pregnancy must be safe and should not cross the placental barrier. The drugs also need to exhibit strong targeting abilities for achieving localized drug release and avoiding maternal and fetal damage resulting from systemic circulation.

Curcumin (Cur) is one of the major components in the rhizomes of turmeric and is known for its anti-inflammatory and antioxidant properties. Cur can directly neutralize free radicals (*e.g.*, reactive oxygen species (ROS) and reactive nitrogen species (RNS)) both *in vitro* and *in vivo*. It can also maintain various antioxidant enzyme activities, such as superoxide dismutase (SOD), catalase (CAT), and glutathione peroxidase (GSH), which play a crucial role in regulating oxidative stress in various diseases.[20–22] However, suboptimal sample preparation and analysis methodologies often hamper the accurate evaluation of bioactivities and their clinical efficacy.[23] Poly (lactic-co-glycolic acid) (PLGA) is a United States Food and Drug Administration (FDA) approved polymer. With its biodegradability, excellent biocompatibility, structural modifiability, and controllable drug release speed, PLGA is widely used in the drug delivery field.[24–27] However, it is difficult to control the intracellular delivery to target organelles.[28]

In our study, we designed biomimetic platelet membrane-loaded nanomaterials, mimicking nanoscale platelets, with robust innate targeting capabilities.[29] We encapsulated curcumin (Cur) and perfluoropentane (PFP) into PLGA, followed by coating with a platelet membrane. Then, we enhanced the delivery of therapeutic agents to venous thrombosis using the phase transition of PFP under the guidance of ultrasound (US) and stimulation with low-intensity focused ultrasound (LIFU). PFP, which is a novel ultrasound contrast agent, undergoes a liquid-to-gas transition and creates microbubbles when subjected to external stimuli.[30] This leads to acoustic droplet vaporization (ADV), exploiting the cavitation effect to dissolve venous thrombi, resulting in a significant diagnostic and therapeutic effect[31] (Fig. 1). The early diagnosis of thrombus is restricted by the inherent shortcomings of traditional imaging techniques in clinic.[32] US has decreased diagnostic reliability in the cases of obese pregnant women, significant limb swelling, small thrombus volumes, and deep vascular locations. However, the nanomaterials we designed underwent a phase transition and generated high-echo microbubbles, enhancing ultrasound signals and further improving the accuracy and sensitivity of venous thrombosis diagnosis. Based on this, we aim to establish a multifunctional molecular imaging therapy that integrates superior biocompatibility and targeting capability for early diagnosis, precise treatment, and efficacious monitoring of pregnancy-related venous thrombosis. Moreover, the therapy is a targeted drug delivery system. It is possible to detect specific molecular changes at the organ, cellular, and even subcellular levels in a living state, while also guiding disease treatment at the molecular level.[33–35]

The vascular endothelium has several important functions, including hemostasis.[36] In the process of thrombus formation and thrombolysis, endothelial damage occurs, leading to platelet activation and an excessive generation of ROS, intensifying oxidative stress. This further promotes platelet activation and aggregation and triggers the overexpression of inflammatory factors, worsening the condition of damaged blood vessels and increasing the risk of recurrent venous thrombosis.[37] To improve the microenvironment of damaged blood vessels, our nanomaterials release curcumin directly to the site of vascular lesions, clearing ROS. Curcumin reacts with hydrogen peroxide (H_2O_2) in the thrombotic area to produce oxygen (O_2) while inhibiting pro-inflammatory mediators, cytokines, and inflammatory signaling pathways. This improvement in the vascular microenvironment prevents the reformation of thrombi, further enhancing the efficacy of thrombosis treatment.

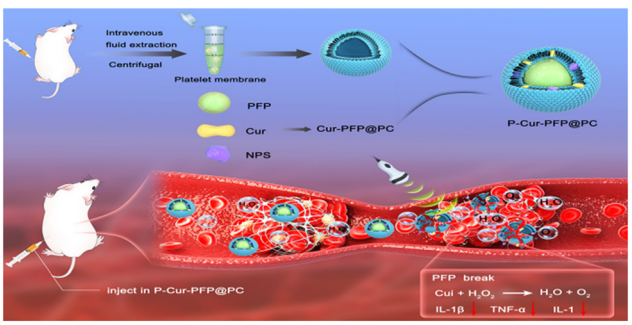

Fig. 1 Scheme for P-Cur–PFP@PC nanodroplet synthesis and illustration of P-Cur–PFP@PC-mediated specific therapy.

2. Results and discussion

2.1 Synthesis and characterization of P-Cur–PFP@PC nanomaterials

We synthesized Cur–PFP@PC using the emulsion solvent evaporation method, combining platelet membrane vesicles (PMV) with Cur–PFP@PC to create platelet membrane-coated nanomaterial named P-Cur–PFP@PC. Transmission electron microscopy (TEM) revealed the spherical nature of the prepared nanomaterials, with P-Cur–PFP@PC displaying a noticeable core–shell structure compared to Cur–PFP@PC (Fig. 2A). Dynamic light scattering (DLS) showed that the average hydrodynamic diameter of Cur–PFP@PC was 234.3 ± 8.63 nm while that of P-Cur–PFP@PC was 267 ± 2.61 nm, indicating an increase in particle size upon PMV coating ($P < 0.0001$) (Fig. 2B). Additionally, the zeta potential changed from −5.86 ± 0.97 mV to −17.95 ± 1.98 mV ($P < 0.0001$) (Fig. 2C). The above TEM size and zeta potential results indicate successful outer membrane coating, consistent with previous reports.

To confirm that the outer membrane was platelet membrane, we validated the presence of functional proteins on the nanomaterials. The results showed that the protein bands of P-Cur–PFP@PC were consistent with PLT protein bands, indicating that P-Cur–PFP@PC inherited protein components

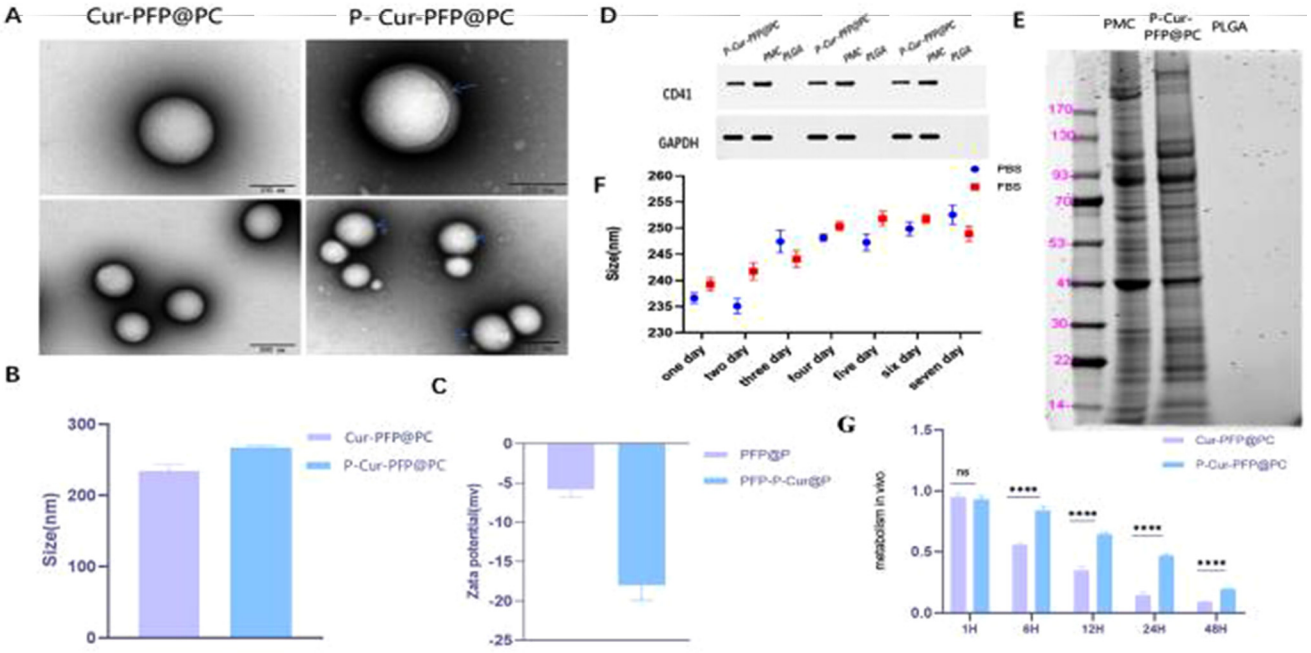

Fig. 2 Design of nanodroplet and its characterization. (A) TEM images of Cur–PFP@PC and P-Cur–PFP@PC. (B) The sizes of Cur–PFP@PC and P-Cur–PFP@PC. (C) The zeta potentials of Cur–PFP@PC and P-Cur–PFP@PC. (D) Western blot analysis of CD41 and GAPDH in platelets, Cur–PFP@PC and P-Cur–PFP@PC. (E) SDS-PAGE gel electrophoresis of platelets, Cur–PFP@PC and P-Cur–PFP@PC. (F) The stability of P-Cur–PFP@PC in PBS and FBS. (G) Fluorescence microplate analysis of the metabolic rate in pregnant mice, $^{****}P < 0.0001$ ($n = 3$).

from the platelet membrane while the PLGA had no PLT protein (Fig. 2D). Meantime, SDS-PAGE gel electrophoresis verified the retention of platelet membrane proteins on P-Cur–PFP@PC nanomaterials, revealing that, although P-Cur–PFP@PC showed weaker protein bands, it shared identical protein components with platelet membranes, while Cur–PFP@PC had no protein components (Fig. 2E). These results further confirmed that the outer transparent membrane of P-Cur–PFP@PC nanomaterials was the platelet membrane.

Next, we characterized the material's particle size, stability, drug loading capacity, and long circulation period *in vivo*. The P-Cur–PFP@PC was placed in PBS and fetal bovine serum for 7 days, and the particle size remained at approximately 250 nm, with no significant changes, demonstrating excellent stability (Fig. 2F). The encapsulation efficiency of Cur was 70.87 ± 0.15% and the drug loading was 8.50 ± 0.02%. We compared the metabolic rates of Cur–PFP@PC and P-Cur–PFP@PC in pregnant mice: P-Cur–PFP@PC had longer circulation than Cur–PFP@PC. The two nanomaterials showed an obvious difference in metabolic rate starting at 6 hours (Fig. 2G). In summary, we successfully prepared biomimetic platelet membrane-loaded curcumin nanomaterials (P-Cur–PFP@PC) which exhibited advantageous stability and drug-loading capabilities and superior circulation.

2.2 Phase transition characteristics and imaging evaluation of P-CUR–PFP@PC nanomaterials

In order to further observe the ADV effect of PFP, we conducted observations under an optical microscope (Fig. 3A). With increasing LIFU irradiation time, the volume began to significantly increase at 5 minutes, reaching its maximum at 10 minutes. After 15 minutes, it gradually decreased and ruptured. This change in morphology clearly exhibited the LIFU-induced phase transition of the nanomaterials. Furthermore, we observed the ultrasound signals of P-Cur–PFP@PC in both brightness-mode ultrasound (B Mode) and contrast-enhanced ultrasound (CEUS) (Fig. 3B). The microbubbles gradually increased, and the ultrasound signal progressively strengthened. At 10 minutes, the signal reached its peak, providing the clearest imaging. Based on this, we hypothesized that the application of LIFU irradiation induced phase transition and released microbubbles when P-Cur–PFP@PC effectively targeted the thrombus and accumulated. Then, it resulted in an increased ultrasound signal at the thrombus site, compensating for the shortcomings of traditional imaging, which can be compromised by external conditions. We injected saline, Cur, Cur–PFP@PC and P-Cur–PFP@PC separately into mice with venous thrombosis. After LIFU irradiation, the results displayed a significantly enhanced ultrasound signal in the P-Cur–PFP@PC group, as expected, and the other groups showed weaker ultrasound signals (Fig. 3C).

2.3 Safety evaluation of nanomaterials

To assess the cell viability, HUVECs cells were incubated with different concentrations of P-Cur–PFP@PC and Cur–PFP@PC nanomaterials, separately, for 12 hours. Cell viability remained nearly 100% at all concentrations (Fig. 4A), indicating that

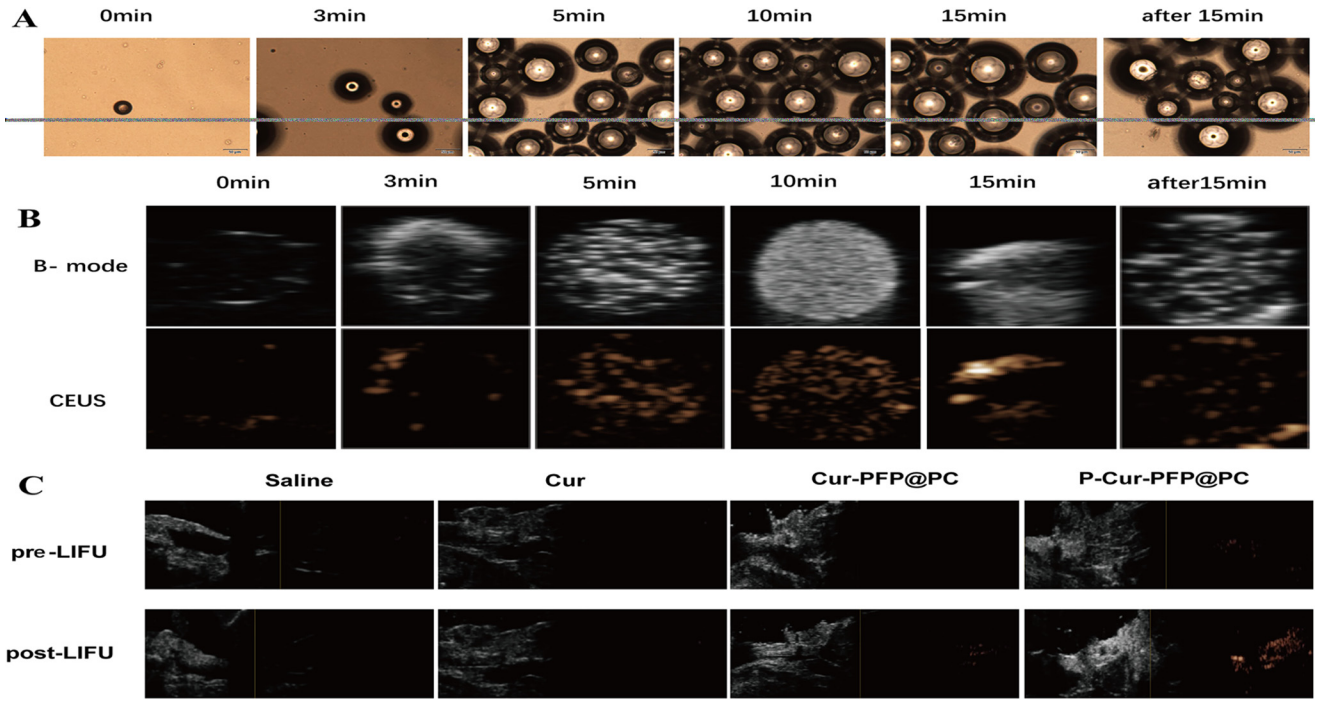

Fig. 3 Phase transition of nanomaterials *in vitro* and US images *in vivo*. (A) Optical microscopy images of P-Cur–PFP@PC after LIFU irradiation at different timepoints. Scale bar = 50 μm. (B) US images (B-mode and CEUS) of P-Cur–PFP@PC at different timepoints with LIFU irradiation *in vitro*. (C) US images (B-mode and CEUS) of the saline, Cur, Cur–PFP@PC and P-Cur–PFP@PC before and after LIFU irradiation *in vivo* (n = 3).

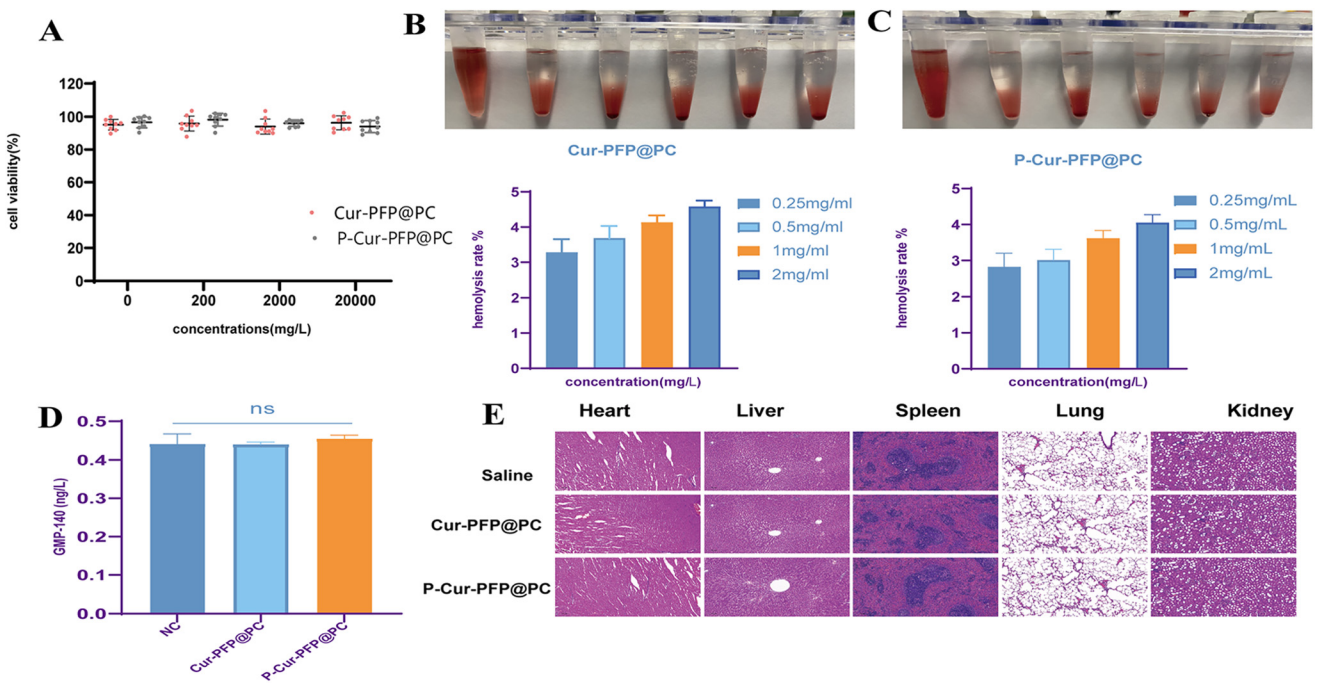

Fig. 4 The safety of nanomaterials. (A) Effects of Cur–PFP@PC and P-Cur–PFP@PC on HUVEC cells at the indicated drug concentration. (B and C) Hemolysis rates of different concentrations of Cur–PFP@PC and P-Cur–PFP@PC. (D) Platelet aggregation rates of saline, Cur–PFP@PC and P-Cur–PFP@PC. (E) H&E staining of the heart, liver, spleen, lung, and kidney of ICR rats after different treatments. Scale bar = 100 μm (n = 4).

these nanomaterials are benign to normal cells, even at higher concentrations (20 000 mg L^{-1}).

In addition, we conducted a hemolysis rate test *in vitro*. A 2% red blood cell suspension in PBS was collected, and different concentrations of P-Cur–PFP@PC and Cur–PFP@PC nanomaterials (0.25 mg mL^{-1}, 0.5 mg mL^{-1}, 1 mg mL^{-1}, 2 mg mL^{-1}) were co-incubated for 4 hours. Hemolysis rates were measured using an enzyme-linked immunosorbent, and the

results are shown in Fig. 4B and C. Hemolysis rates at different concentrations remained within the normal range, demonstrating that these nanomaterials possess excellent biocompatibility and absence of hemolysis *in vitro*.

After incubating mouse whole blood with P-Cur–PFP@PC and Cur–PFP@PC nanomaterials, platelet aggregation testing was performed (Fig. 4D). In comparison to the saline control group, neither of these nanomaterials activated platelets, mitigating the risk of thrombus formation.

To confirm the safety of the nanomaterials *in vivo*, P-Cur–PFP@PC and Cur–PFP@PC nanomaterials were intravenously injected into mice at three times the therapeutic doses. Mice in the control group received saline. After 7 days, the organs (heart, liver, spleen, lung and kidney) were harvested, and their HE-stained sections indicated no structural changes in the nanomaterial-treated groups compared to the control group, suggesting that these nanomaterials are safe *in vivo* (Fig. 4E).

2.4 Targeting capability evaluation of the nanomaterials

To evaluate the targeting capability of the nanomaterials *in vitro*, HUVEC cells were incubated with Dil-labeled P-Cur–PFP@PC (Dil-P-Cur–PFP@PC) and Cur–PFP@PC (Dil-Cur–PFP@PC). The Dil-P-Cur–PFP@PC with red fluorescence exhibited excellent co-localization with platelets under a confocal fiber optic microscope, significantly outperforming Dil-Cur–PFP@PC, indicating that the platelet membrane on the surface of P-Cur–PFP@PC displayed remarkable targeting capability (Fig. 5A).

To detect the phagocytosis of HUVECs on Dil-P-Cur–PFP@PC and Dil-Cur–PFP@PC, 2×10^5 HUVEC cells were seeded in each well of a 6-well plate and cultured for 24 hours. Dil-P-Cur–PFP@PC and Dil-Cur–PFP@PC nanomaterials were added, with PBS as the control. The cells were incubated for 1, 2, 4, and 6 hours, followed by flow cytometry analysis after digestion. The cell phagocytic capacity strengthened over time until reaching its peak at 4 hours before gradually declining. The ability of cells to phagocytize Dil-P-Cur–PFP@PC was significantly superior to that for Dil-Cur–PFP@PC (Fig. 5B). These results were consistent with the confocal microscopy results, indicating the superior targeting capacity of the Dil-P-Cur–PFP@PC nanomaterial.

We conducted a targeting evaluation of these nanomaterials in ICR mice on the 13.5th day of pregnancy. Damage to endothelial cells in the inferior vena cava was induced using $FeCl_3$, resulting in thrombus formation (thrombus group). Subsequently, Dil-P-Cur–PFP@PC and Dil-Cur–PFP@PC were injected into the tail vein. After 5 minutes, frozen sections of venous thrombi were stained with CD42. The targeting nanomaterials (in red in Fig. 5C) exhibited excellent co-localization with fibrin (in green) within the thrombus, while the Dil-Cur–PFP@PC group displayed significantly weaker co-localization than Dil-P-Cur–PFP@PC group (Fig. 5C). These findings demonstrated the effective targeting of thrombi by the targeting nanomaterial, indicating its potential for targeted thrombolysis.

2.5 Thrombolysis assessment of nanomaterials

Rat venous blood was collected and allowed to form clots at room temperature. Six experimental groups were established

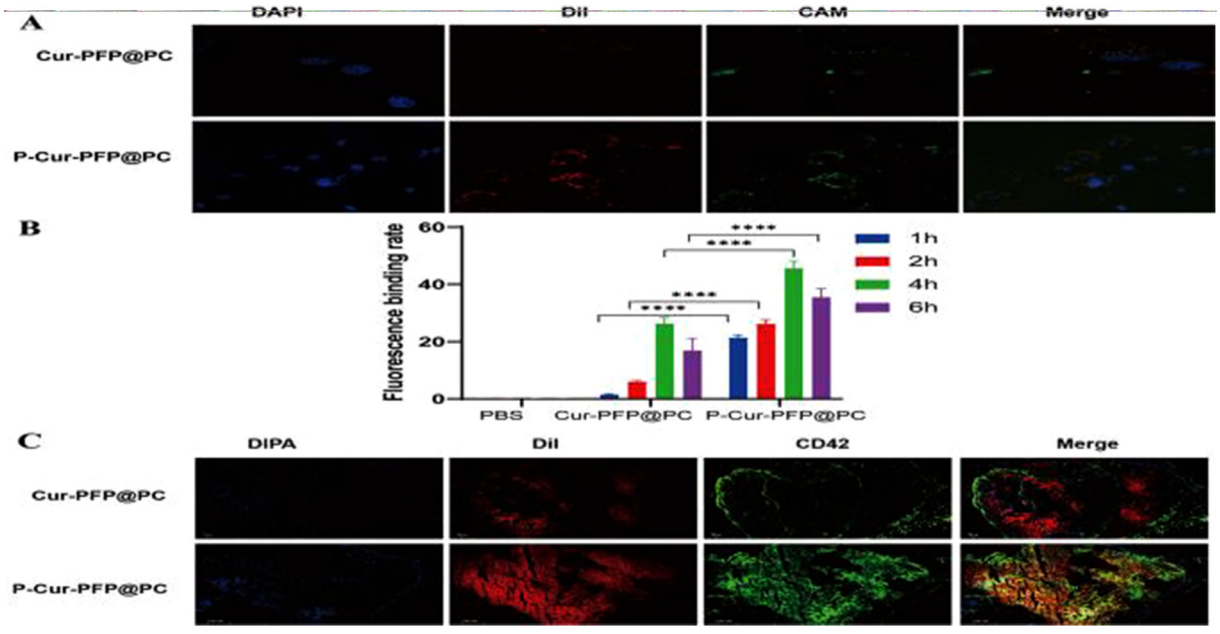

Fig. 5 Targeting of nanomaterials *in vivo* and *in vitro*. (A) Confocal microscopy analysis of the targeting of Cur–PFP@PC and P-Cur–PFP@PC to activated platelets. Nuclei were stained with DIPA (blue), Cur–PFP@PC and P-Cur–PFP@PC were labeled with Dil (red), while platelets were labeled with Calcein-AM (green). Scale bar: 10 μm. (B) The flow cytometry test results of Cur–PFP@PC and P-Cur–PFP@PC at different timepoints, ****P < 0.0001. (C) Frozen section analysis of the targeting of Cur–PFP@PC and P-Cur–PFP@PC to thrombus *in vivo*. Nuclei were stained with DIPA (blue), Cur–PFP@PC and P-Cur–PFP@PC were labeled with Dil (red) and thrombi were labeled with CD42 (green). Scale bar: 500 μm (n = 3).

(PBS group, Cur group, Cur–PFP@PC group, P-Cur–PFP@PC group, Cur–PFP@PC + LIFU group, P-Cur–PFP@PC + LIFU group). The clot weight was measured every 5 minutes and, after 60 minutes, confocal laser scanning microscopy was performed. As shown in Fig. 6A and B, the weight of clots in the LIFU irradiation groups was reduced compared to the non-LIFU groups. Among the LIFU groups, the thrombolysis effect of P-Cur–PFP@PC + LIFU was superior to that of Cur–PFP@PC + LIFU. There was no significant change in clot weight among the non-LIFU groups, and the results were consistent with the measurements. The differences among the non-LIFU groups were not statistically significant, while the differences among the LIFU groups were statistically significant ($P < 0.0001$). Additionally, a significantly loose fibrin mesh was observed in the LIFU groups by confocal scanning electron microscopy (Fig. 6C).

We conducted a thrombolysis ability assessment in pregnant ICR mice, successfully modeling inferior vena cava thrombosis. The mice were injected with 200 μL of saline, Cur (5 mg ml^{-1}), Dil-Cur–PFP@PC (5 mg ml^{-1}, 200 μL) or Dil-P-Cur–PFP@PC (5 mg ml^{-1}, 200 μL) through tail veins. Then, the mice were given 10 minutes of LIFU radiation, and the thrombus volume of each group was detected by B mode. The control group and Cur group exhibited a gradual increase in thrombus volume over time, the Dil-Cur–PFP@PC group showed a slight reduction in thrombus volume compared to before LIFU radiation, and the Dil-P-Cur–PFP@PC group displayed a significant reduction in thrombus size (Fig. 7A). Comparing the HE stained thrombus from each group, the non-LIFU groups exhibited relatively poorer thrombolysis compared to the LIFU groups, while the Dil-P-Cur–PFP@PC + LIFU group displayed the best effect of thrombolysis (Fig. 7B), consistent with observations made by the ultrasound imaging system.

2.6 ROS clearance effect assessment of nanomaterials

To validate the ROS clearance effect of Cur *in vitro*, we used PBS as a control group to assess the ability of Cur to clear superoxide radicals, singlet oxygen, and hydroxyl radicals. As shown in Fig. 8A–C, Cur exhibited a noticeable ROS clearance effect compared to PBS. We incubated HUVEC cells with different groups as previously mentioned, detected intracellular ROS, and observed the fluorescence signal by fluorescence microscope (Fig. 8D). The LIFU groups exhibited a stronger ROS clearance ability within the cells compared to the non-LIFU groups. Quantitative analysis using a fluorescence microplate reader showed a significant ROS clearance effect in the LIFU groups compared to the non-LIFU groups (Fig. 8E). There was no statistically significant difference between P-Cur–PFP@PC + LIFU and Cur–PFP@PC + LIFU. Notably, despite the lack of strong targeting in the Cur–PFP@PC group, all the nanomaterials were dissolved in the cell culture medium and, constrained by the space of six-well plate, underwent phase transition under LIFU radiation, achieving acoustic droplet vaporization (ADV) and allowing Cur to enter the cells for ROS clearance. In contrast, the lower dissolution of free Cur limited its efficiency in entering the cytoplasm for ROS clearance. This further validated the hydrophobicity and instability of Cur directly impacting its clinical trials, and the nanomaterials we prepared successfully address these issues, making them suitable for clinical trials.

Moreover, we evaluated the ROS clearance of nanomaterials in successfully modeled ICR pregnant mice. From the 13.5th

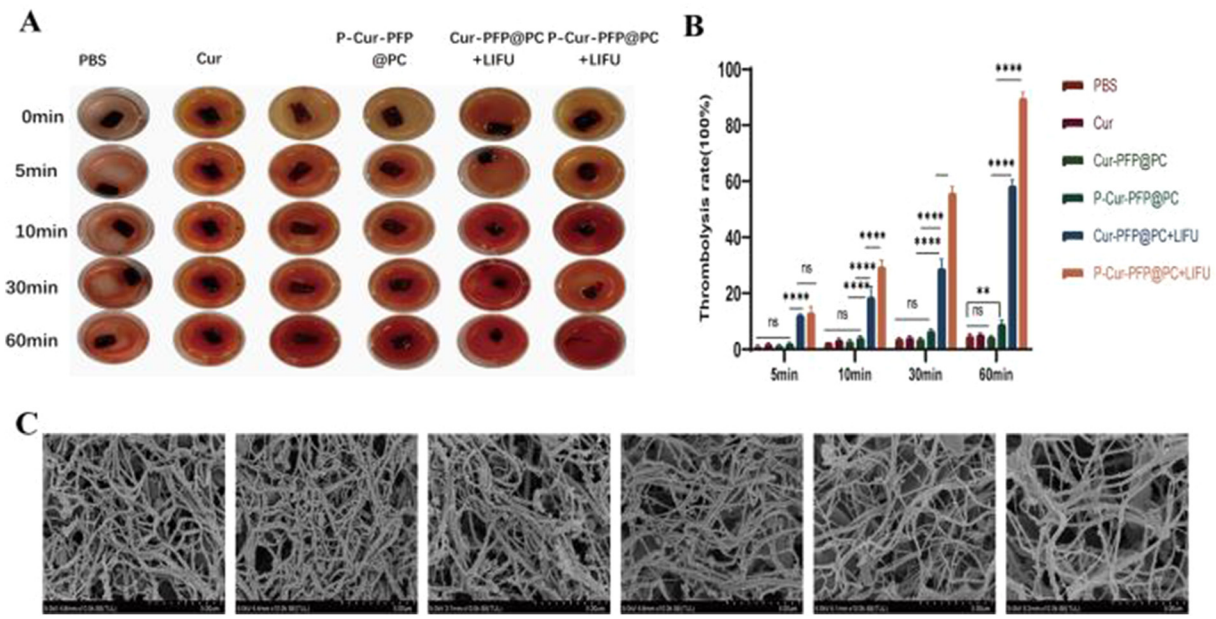

Fig. 6 Thrombolysis *in vitro*. (A) The appearance of a thrombus (digital photograph) after incubation with PBS, Cur, Cur–PFP@PC, P-Cur–PFP@PC, Cur–PFP@PC + LIFU and P-Cur–PFP@PC + LIFU (7 W cm^{-2} LIFU irradiation) at different timepoints. (B) The weight of thrombus clots of each group (values are means ± sd, ****$P < 0.0001$). (C) SEM analysis of fibrin mesh in each group. Scale bar: 10 μm.

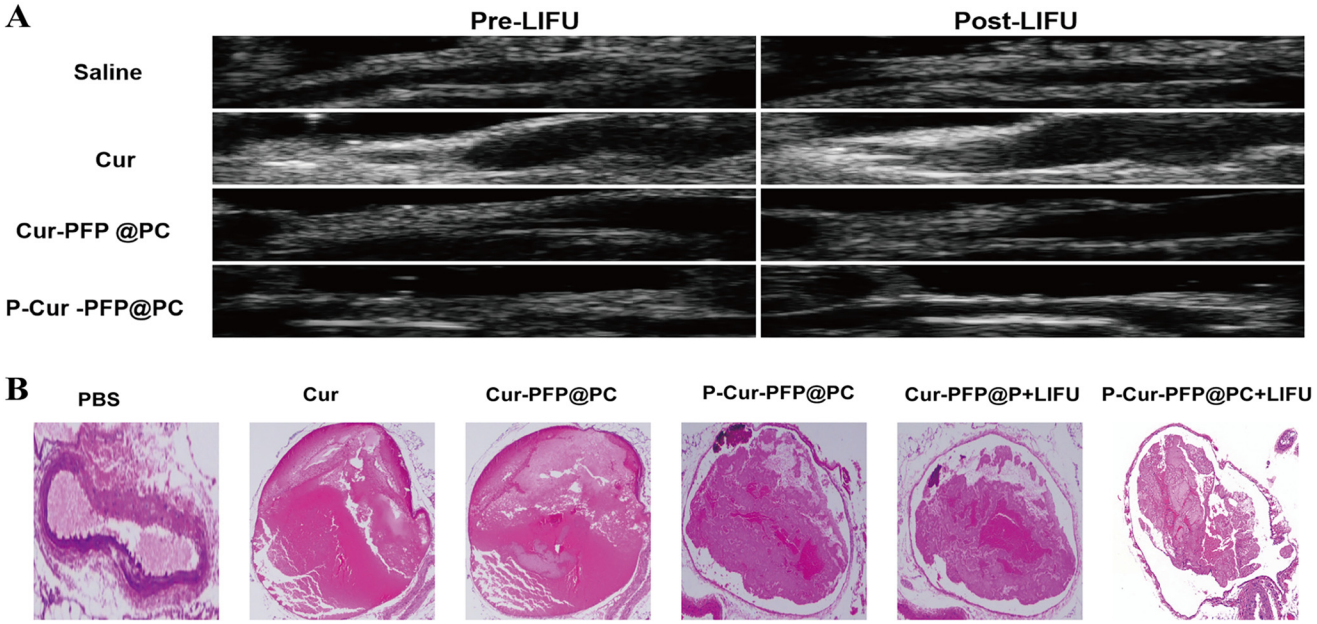

Fig. 7 Thrombolysis *in vivo*. (A) Thrombolytic effect in US images (B-mode) of the saline, Cur, Cur–PFP@PC, and P-Cur–PFP@PC before and after LIFU irradiation *in vivo*. (B) H&E staining of the postcava after different treatments (n = 4).

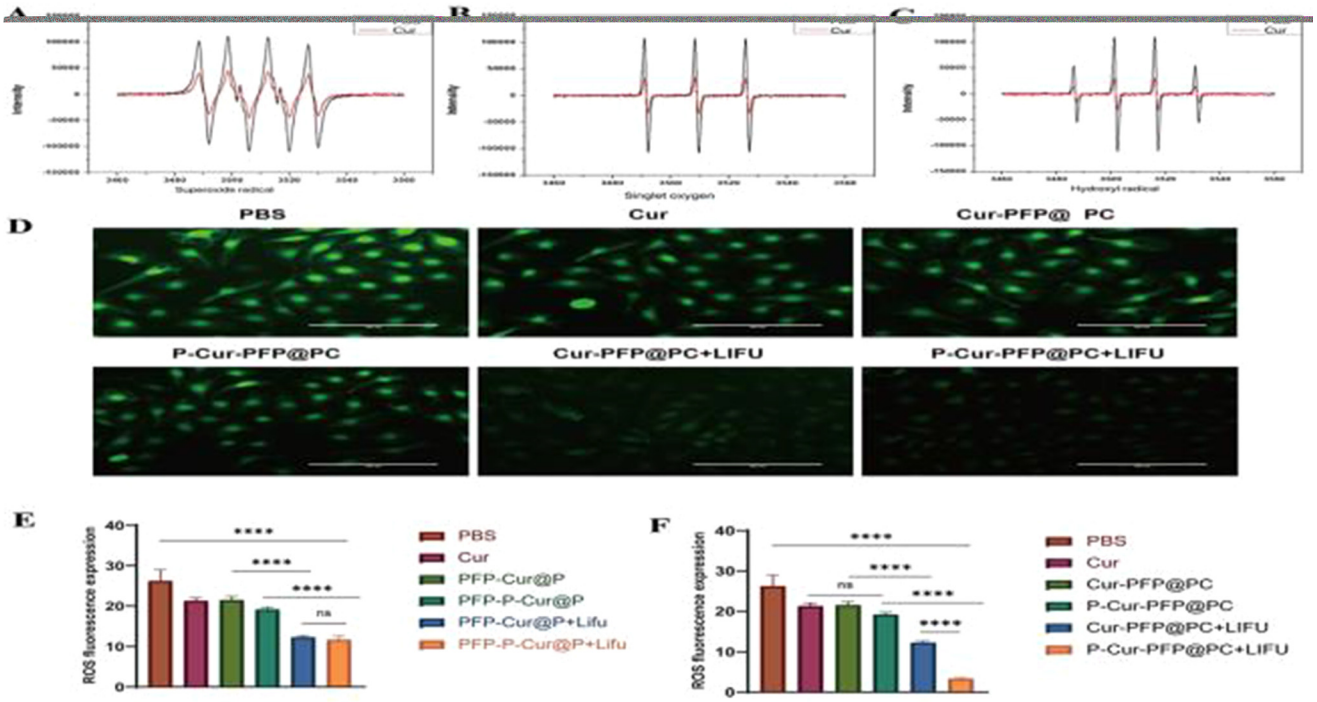

Fig. 8 Clearance of ROS *in vivo* and *in vitro*. (A–C) The scavenging effect of PBS and Cur on ROS. (D) Fluorescence microscopy analysis of free clearance of oxygen from the cell. Scale bar: 200 μm. (E) Quantitative analysis of intracellular ROS clearance, ****P < 0.0001. (F) Detection kit analysis of ROS clearance *in vivo*, ****P < 0.0001.

day of pregnancy, daily tail vein injections of saline, Cur, Cur–PFP@PC, or P-Cur–PFP@PC (5 mg ml^{-1}, 200 μL) were administered. The last two groups received 5 minutes of LIFU radiation at the site of the thrombus. After 4 days of treatment, the thrombus was extracted from the sudden death mice, and parts of the thrombus were subjected to tissue ROS testing using a detection kit. The results indicated that the P-Cur–PFP@PC + LIFU group exhibited the most prominent ROS

clearance effect (Fig. 8F), suggesting that the Cur loaded in nanomaterials can successfully reach the site of the thrombus, undergo targeted release, and effectively eliminate oxygen radicals.

2.7 Detection of inhibition of inflammatory cell infiltration of nanomaterials

To detect the inhibition of inflammatory cell infiltration, endothelial cell damage was induced in HUVEC cells by culturing in a hypoxia incubator for 24 hours. Cells were divided into 6 groups as mentioned previously, with PBS as the control group. The cell supernatant was collected after 24 hours incubation, and the expression levels of the inflammatory factors of each group, IL-1, IL-6, and TNF-α, were measured by ELISA kit (Fig. 9A–C). The control group had the highest expression levels of inflammatory factors, while the P-Cur–PFP@PC + LIFU group had the lowest expression levels, followed by the Cur–PFP@PC + LIFU group. The inter-group differences were statistically significant ($P < 0.0001$).

2.8 Assessment of promotion of HUVEC migration

HUVEC cells were cultured in the condition of hypoxia for 24 hours and subjected to a scratch test using a 200 μL pipette tip. Cells were divided and treated in 6 groups, as described previously, and the migration was observed at 24 hours by inverted microscope (Fig. 9D and E). The P-Cur–PFP@PC + LIFU group demonstrated a superior migratory effect, facilitating the repair of damaged endothelial cells and promoting the healing of damaged blood vessels.

2.9 Post-treatment safety assessment *in vivo*

After the formation of inferior vena cava thrombosis in pregnant ICR mice, 3-fold treatment doses of P-Cur–PFP@PC and Cur–PFP@PC nanomaterials were administered to pregnant ICR mice starting on the 8.5th day of pregnancy, and the control group consisted of non-thrombotic pregnant mice injected with saline. The LIFU group received daily 5-minute LIFU radiation treatment until the 16.5th day of pregnancy. Eye blood samples were collected for hematological, biochemical, and coagulation function tests, and all groups exhibited results within the normal range (Fig. 10A–F). The weights of the fetal mouse and placenta were recorded (Fig. 10G). The P-Cur–PFP@PC + LIFU group had a significantly greater increase in fetal mouse weight compared to the other groups, with statistically significant inter-group differences ($P < 0.0001$), but the results of placental weight showed no difference. We speculate that the basal weight of the placenta is light, while the change is expressed at the molecular level. Additionally, the HE stained organs from the fetal mouse fed until 4 weeks showed no abnormalities (Fig. 10H). In summary, our nanomaterial not only has a therapeutic effect on thrombosis but also has a high level of safety, with no adverse effects on pregnant mice and their offspring.

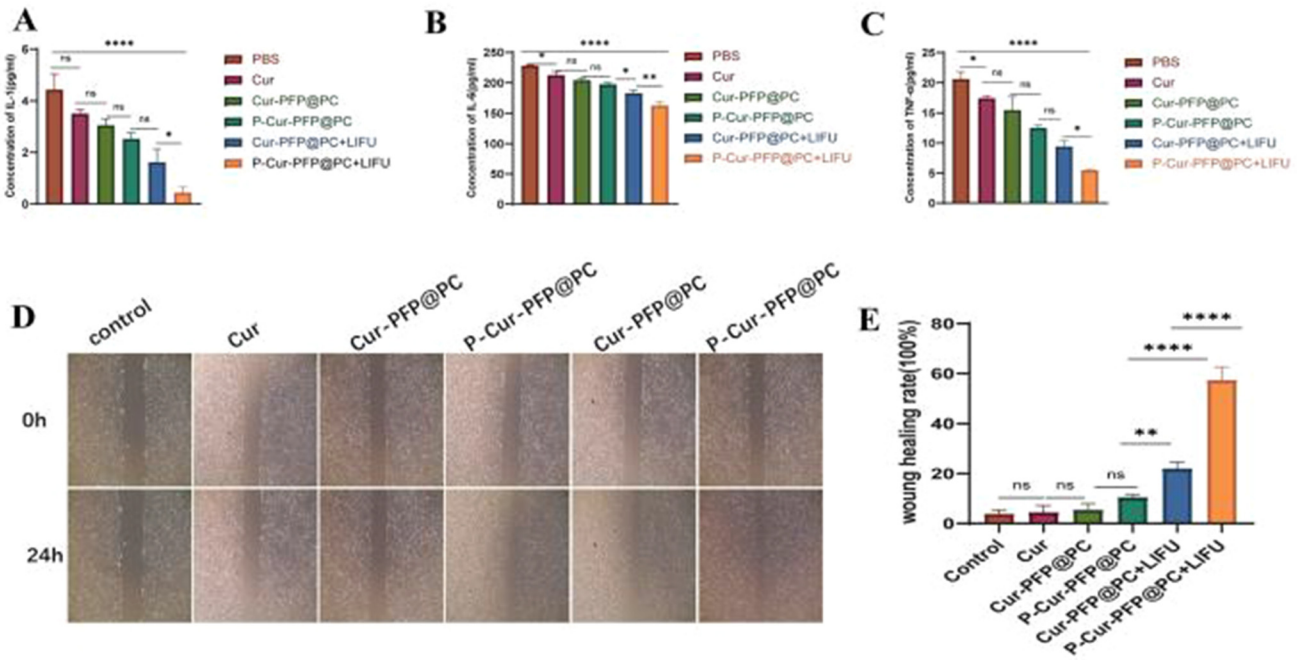

Fig. 9 Expression of inflammatory factors after therapy and cell repair. (A–C) Elisa kit analysis of IL-1, IL-6, and TNF-α in cells in each group, ****$P < 0.0001$. (D) Images and healing rates from the wound healing assay after separate incubation with PBS, Cur, Cur–PFP@PC, P-Cur–PFP@PC, and the last two groups with added LIFU (7 W cm^{-2} LIFU irradiation) for 24 h. Scale bar: 20 μm. Values are mean ± sd, ****$P < 0.0001$ ($n = 3$). (E) Quantitative analysis of wound healing rates (100%) in different groups.

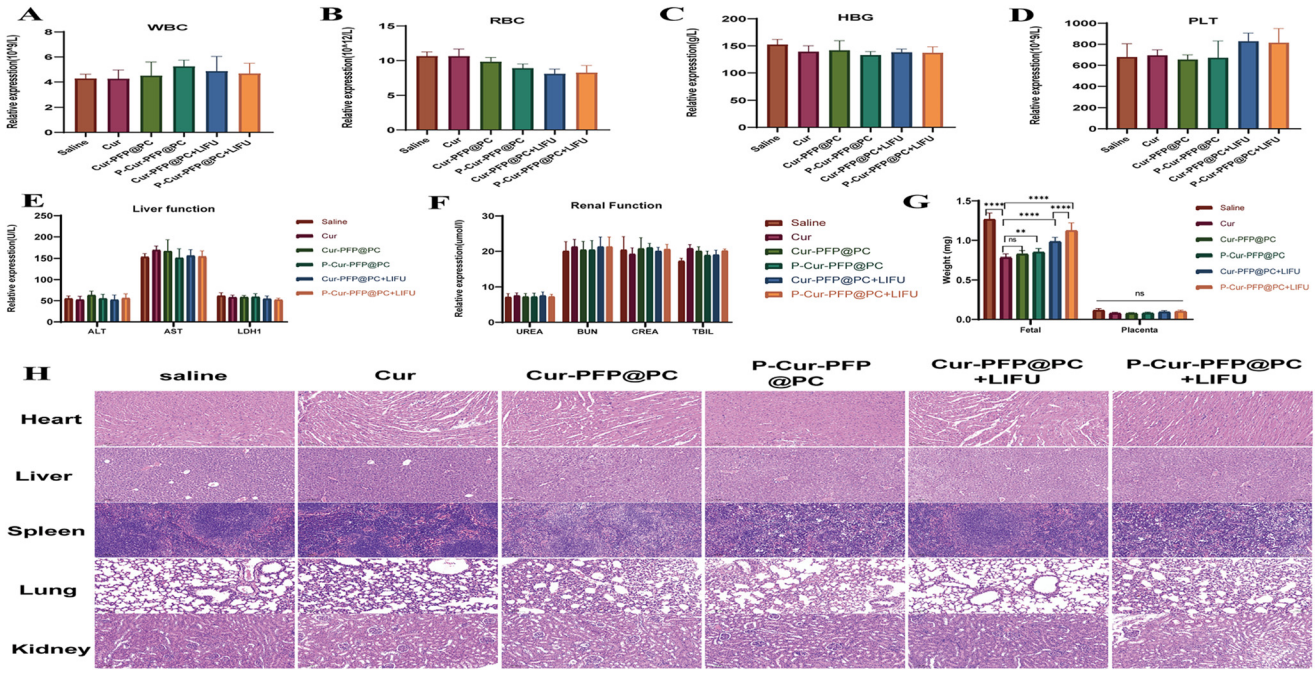

Fig. 10 Security detection *in vivo*. (A–F) Biochemical detection of WBC, RBC, PLT, liver function and renal function in ICR mice after therapy. (G) The weight of fetal mouse and placenta in each group. Values are means ± sd, ****$P < 0.0001$. (H) H&E staining of the offspring mice in heart, liver, spleen, lung and kidney after different treatments ($n = 4$).

3. Conclusions

The main factors contributing to venous thrombosis during pregnancy are elevated estrogen levels, heightened blood coagulation state, advanced maternal age, cesarean section, prolonged bed rest, reduced blood flow, multiple pregnancies, uterine compression, obstructed inferior vena cava return, preeclampsia, the release of coagulation enzymes, and increased coagulation activity. Currently, there are no non-invasive, safe, and reliable clinical trials available for this condition. Moreover, traditional imaging methods have limitations in diagnosing venous thrombosis in pregnant women.

In our study, we developed a novel approach by involving the encapsulation of nanomaterials with platelet membranes. This allowed the nanomaterials to directly mimic the characteristics of source cells, replicating highly complex biological functions on their surface. As a result, they exhibited prolonged circulation in the bloodstream, excellent biocompatibility, and precise targeting, thus resolving the issues of previous molecular probes, such as inadequate binding and targeting abilities in the context of venous thrombosis. Once the thrombus was specifically captured by the platelet membrane-encapsulated nanomaterials and exposed to LIFU irradiation, the cavitation effect was utilized to damage the internal structure of the thrombus, increasing its sensitivity to dissolution, and enabling profound thrombus resolution. Moreover, LIFU exhibited thrombus-specific characteristics, allowing for localized thrombus treatment without the requirement for systemic anticoagulant therapy, thereby reducing the side effects of prolonged medication.[31] Furthermore, the microbubbles generated during this process enhance ultrasound imaging signals, facilitating visual thrombolysis, ensuring precise localization, controlling drug release, improving the damaged vascular microenvironment, repairing injured vessels, and reducing the risk of recurrent thrombosis.

This nanomaterial exhibited excellent safety and offered a solution to the systemic side effects associated with the treatment of venous thrombosis during pregnancy. However, the microenvironment of thrombotic diseases is unknown.[37] We have designed a safe and thrombin-free material, guided by B-ultrasound imaging, to destroy thrombus under LIFU irradiation, while generating bubbles that can increase ultrasound imaging contrast and solve the difficult problem of imaging obese pregnant women. Precise drug release at the thrombus site to repair damaged blood vessels and highly localized treatment of venous thrombosis during pregnancy is very beneficial, perfectly avoiding the long-term systemic drug treatment that can cause maternal and infant injury.

4. Experimental section

4.1 Synthesis of Cur–PFP@PC

50 mg of PLGA powder and 10 mg curcumin were weighed and dissolved in 2 ml of dichloromethane with sonication. Then, 200 μl of PFP was added, and sonication was performed on ice at a frequency of 5/5 seconds with a power of 45% using a sonicator for 4 minutes. Subsequently, 8 ml of 4% PVA and 10 ml

of 2% isopropanol were added, followed by sonication at a frequency of 5/5 seconds and 30% power for 2 minutes and 30 seconds. Magnetic stirring was conducted in a 4 °C ice bath for 3 hours, followed by centrifugation at 10 000 r in a 4 °C low-temperature centrifuge for 5 minutes.

Synthesis of P-Cur–PFP@PC: 1 ml of 5 mg ml^{-1} prepared Cur–PFP@PC was taken and mixed with the extracted platelet membrane. Sonication was performed at 30% power and a frequency of 5/5 seconds for 2 minutes and 30 seconds.

Characterization of P-Cur–PFP@PC Nanomaterial: TEM (Hitachi H-7600, Japan) was used to obtain the morphology of the prepared P-Cur–PFP@PC, while SEM (scanning electron microscopy) was used to examine the structure of the platelet membranes. Platelet membrane extraction was confirmed using western blot (WB) and Coomassie blue staining. The zeta potential and average particle size of Cur–PFP@PC and P-CUR–PFP@PC were measured using a dynamic light scattering instrument (DSL, Brookhaven Instruments ZEN3600, USA).

Mice and Cells: ICR mice (6 weeks old) were purchased from Chongqing Enbi Biological Technology Co., Ltd. All mice were fed under IVC-level conditions in the Chongqing Medical University animal facility, and all animal experiments strictly adhered to the compliance standards of the Institutional Animal Care and Use Committee.

All animal-handling procedures were performed according to the Guide for the Care and Use of Laboratory Animals of the Chinese Association for Laboratory Animal Sciences and followed the guidelines of the Animal Welfare Act. This animal study was approved by the Ethics Committee of the First Affiliated Hospital of Chongqing Medical University (approval number: 2020-790)

HUVEC cells were provided by the Maternal-Fetal Laboratory of the First Affiliated Hospital of Chongqing Medical University, the parameters for the hypoxic culture chamber were set at 37 °C, 1% O_2, 5% CO_2, and 94% N_2.

4.2 Phase transition properties and *in vitro* release of nanomaterials

2 ml of P-Cur–PFP@PC was added to a gelatin model and irradiated with LIFU at an acoustic power of 7 W cm^2. Ultrasound images were collected at different time intervals post-irradiation, using B-mode and CEUS (n = 3).

Author contributions

Lin Xu (Co-first author 1): conceptualization, methodology, formal analysis, writing – original draft, writing – review and editing, project administration. Yijie Zhou (Co-first author 2): formal analysis, investigation, visualization, writing – review and editing. Na Li (Co-first author 3): conceptualization, investigation, date curation, writing – original draft, writing – review and editing, supervision. Hongbo Qi (Corresponding author 1): methodology, software, resources, supervision, project administration, funding acquisition. Anyu Yang (Corresponding author 2): methodology, software, resources, supervision.

Conflicts of interest

The authors report no conflicts of interest in this work.

Acknowledgements

The research is supported by the Key Research Program of Chongqing Science and Technology Bureau (No. CSTB2022TIAD-KPX0156); Chongqing Medical Scientific Research Project (Joint Project of Chongqing Health Commission and Science and Technology Bureau) (2023GGXM005); Joint Funds of the National Natural Science Foundation of China (No. U21A20346); the General Program of Chongqing Science and Technology Bureau (No. cstc2021jcyj-msxm x0374). The authors thank the support from "111 program" of Ministry of Education P.R.C and State Administration of Foreign Experts Affairs P.R.C.

References

1 S. V. Konstantinides, G. Meyer, C. Becattini, H. Bueno, G. J. Geersing, V. P. Harjola, M. V. Huisman, M. Humbert, C. S. Jennings, D. Jiménez, N. Kucher, I. M. Lang, M. Lankeit, R. Lorusso, L. Mazzolai, N. Meneveau, N. Á. Fionnuala, P. Prandoni, P. Pruszczyk, M. Righini, A. Torbicki, E. Van Belle and J. L. Zamorano, 2019 ESC Guidelines for the diagnosis and management of acute pulmonary embolism developed in collaboration with the European Respiratory Society (ERS), *Eur. Heart J.*, 2020, **41**, 543–603.

2 A. A. Creanga, C. Syverson, K. Seed and W. M. Callaghan, Pregnancy-Related Mortality in the United States, 2011-2013, *Obstet. Gynecol.*, 2017, **130**, 366–373.

3 Y. Chen, Y. Dai, J. Song, L. Wei, Y. Ma, N. Tian, Q. Wang, Q. Zhang, Y. Zhang, X. L. Wang, J. Zhang and R. Liu, Establishment of a risk assessment tool for pregnancy-associated venous thromboembolism and its clinical application: protocol for a prospective observational study in Beijing, *BMC Pregnancy Childbirth*, 2019, **19**, 294.

4 M. S. Mosquera and J. A. Diaz, Back To Basics: Theory of Thrombus Formation and Potential Implications for Therapies?, *Tech. Vasc. Interv. Radiol.*, 2023, **26**, 100894.

5 C. Dubois, L. Panicot-Dubois, J. F. Gainor, B. C. Furie and B. Furie, Thrombin-initiated platelet activation in vivo is vWF independent during thrombus formation in a laser injury model, *J. Clin. Invest.*, 2007, **117**, 953–960.

6 P. Zhao, Y. Zhao, Q. Zhang, Z. Zhou, J. Zhou and F. Ruan, Venous Thromboembolism and Ovarian Torsion-detorsion in Pregnancy: a Case Report and Systematic Review of the Literature, 2020, **https://europepmc.org/article/ppr/ppr246915**.

7 N. J. Kassebaum, A. Bertozzi-Villa, M. S. Coggeshall, K. A. Shackelford, C. Steiner, K. R. Heuton, *et al.*, Global, regional, and national levels and causes of maternal mortality during 1990–2013: a systematic analysis for the Global Burden of Disease Study 2013, *Lancet*, 2014, **384**, 980–1004.

8 R. Cantwell, T. Clutton-Brock, G. Cooper, A. Dawson, J. Drife, D. Garrod, A. Harper, D. Hulbert, S. Lucas, J. McClure, H. Millward-Sadler, J. Neilson, C. Nelson-Piercy, J. Norman, C. O'Herlihy, M. Oates, J. Shakespeare, M. de Swiet, C. Williamson, V. Beale, M. Knight, C. Lennox, A. Miller, D. Parmar, J. Rogers and A. Springett, Saving Mothers' Lives: Reviewing maternal deaths to make motherhood safer: 2006-2008. The Eighth Report of the Confidential Enquiries into Maternal Deaths in the United Kingdom, *BJOG*, 2011, **118**, 1–203.

9 A. Zenych, L. Fournier and C. Chauvierre, Nanomedicine progress in thrombolytic therapy, *Biomaterials*, 2020, **258**, 120297.

10 K. M. Nichols, S. Henkin and M. A. Creager, Venous Thromboembolism Associated With Pregnancy: JACC Focus Seminar, *J. Am. Coll. Cardiol.*, 2020, **76**, 2128–2141.

11 H. Gong, Q. Zhang, A. Komarla, S. Wang, Y. Duan, Z. Zhou, F. Chen, R. H. Fang, S. Xu, W. Gao and L. Zhang, Nanomaterial Biointerfacing via Mitochondrial Membrane Coating for Targeted Detoxification and Molecular Detection, *Nano Lett.*, 2021, **21**, 2603–2609.

12 V. Chugh, K. Vijaya Krishna and A. Pandit, Cell Membrane-Coated Mimics: A Methodological Approach for Fabrication, Characterization for Therapeutic Applications, and Challenges for Clinical Translation, *ACS Nano*, 2021, **15**, 17080–17123.

13 T. Kang, Q. Zhu, D. Wei, J. Feng, J. Yao, T. Jiang, Q. Song, X. Wei, H. Chen, X. Gao and J. Chen, Nanoparticles Coated with Neutrophil Membranes Can Effectively Treat Cancer Metastasis, *ACS Nano*, 2017, **11**, 1397–1411.

14 J. G. Piao, L. Wang, F. Gao, Y. Z. You, Y. Xiong and L. Yang, Erythrocyte membrane is an alternative coating to polyethylene glycol for prolonging the circulation lifetime of gold nanocages for photothermal therapy, *ACS Nano*, 2014, **8**, 10414–10425.

15 L. Rao, B. Cai, L. L. Bu, Q. Q. Liao, S. S. Guo, X. Z. Zhao, W. F. Dong and W. Liu, Microfluidic Electroporation-Facilitated Synthesis of Erythrocyte Membrane-Coated Magnetic Nanoparticles for Enhanced Imaging-Guided Cancer Therapy, *ACS Nano*, 2017, **11**, 3496–3505.

16 V. Kozlovskaya, J. F. Alexander, Y. Wang, T. Kuncewicz, X. Liu, B. Godin and E. Kharlampieva, Internalization of red blood cell-mimicking hydrogel capsules with pH-triggered shape responses, *ACS Nano*, 2014, **8**, 5725–5737.

17 Y. Shi and T. Lammers, Combining Nanomedicine and Immunotherapy, *Acc. Chem. Res.*, 2019, **52**, 1543–1554.

18 Y. Lu, C. Li, Q. Chen, P. Liu, Q. Guo, Y. Zhang, X. Chen, Y. Zhang, W. Zhou, D. Liang, Y. Zhang, T. Sun, W. Lu and C. Jiang, Microthrombus-Targeting Micelles for Neurovascular Remodeling and Enhanced Microcirculatory Perfusion in Acute Ischemic Stroke, *Adv. Mater.*, 2019, **31**, e1808361.

19 J. Xu, Y. Zhang, J. Xu, G. Liu, C. Di, X. Zhao, X. Li, Y. Li, N. Pang, C. Yang, Y. Li, B. Li, Z. Lu, M. Wang, K. Dai, R. Yan, S. Li and G. Nie, Engineered Nanoplatelets for Targeted Delivery of Plasminogen Activators to Reverse Thrombus in Multiple Mouse Thrombosis Models, *Adv. Mater.*, 2020, **32**, e1905145.

20 J. Estelrich and M. A. Busquets, Prussian Blue: A Nanozyme with Versatile Catalytic Properties, *Int. J. Mol. Sci.*, 2021, **22**, 5993.

21 Y. Gao, G. Yu, K. Xing, D. Gorin, Y. Kotelevtsev, W. Tong and Z. Mao, Finely tuned Prussian blue-based nanoparticles and their application in disease treatment, *J. Mater. Chem. B*, 2020, **8**, 7121–7134.

22 M. A. Busquets and J. Estelrich, Prussian blue nanoparticles: synthesis, surface modification, and biomedical applications, *Drug Discovery Today*, 2020, **25**, 1431–1443.

23 R. R. Kotha and D. L. Luthria, Curcumin: Biological, Pharmaceutical, Nutraceutical, and Analytical Aspects, *Molecules*, 2019, **24**, 2930.

24 D. N. Kapoor, A. Bhatia, R. Kaur, R. Sharma, G. Kaur and S. Dhawan, PLGA: a unique polymer for drug delivery, *Ther. Delivery*, 2015, **6**, 41–58.

25 F. Sadat Tabatabaei Mirakabad, K. Nejati-Koshki, A. Akbarzadeh, M. R. Yamchi, M. Milani, N. Zarghami, V. Zeighamian, A. Rahimzadeh, S. Alimohammadi, Y. Hanifehpour and S. W. Joo, PLGA-based nanoparticles as cancer drug delivery systems, *Asian Pac. J. Cancer Prev.*, 2014, **15**, 517–535.

26 M. Mir, N. Ahmed and A. U. Rehman, Recent applications of PLGA based nanostructures in drug delivery, *Colloids Surf., B*, 2017, **159**, 217–231.

27 Y. Su, B. Zhang, R. Sun, W. Liu, Q. Zhu, X. Zhang, R. Wang and C. Chen, PLGA-based biodegradable microspheres in drug delivery: recent advances in research and application, *Drug Delivery*, 2021, **28**, 1397–1418.

28 A. Harada, H. Tsutsuki, T. Zhang, R. Lee, K. Yahiro, T. Sawa and T. Niidome, Preparation of Biodegradable PLGA-Nanoparticles Used for pH-Sensitive Intracellular Delivery of an Anti-inflammatory Bacterial Toxin to Macrophages, *Chem. Pharm. Bull.*, 2020, **68**, 363–368.

29 J. Xu, Y. Zhang, J. Xu, G. Liu, C. Di, X. Zhao, X. Li, Y. Li, N. Pang and C. Yang, Engineered nanoplatelets for targeted delivery of plasminogen activators to reverse thrombus in multiple mouse thrombosis models, *Adv. Mater.*, 2020, **32**, 1905145.

30 Z. Yang, J. Yao, J. Wang, C. Zhang, Y. Cao, L. Hao, C. Yang, C. Wu, J. Zhang, Z. Wang, H. Ran and Y. Tian, Ferrite-encapsulated nanoparticles with stable photothermal performance for multimodal imaging-guided atherosclerotic plaque neovascularization therapy, *Biomater. Sci.*, 2021, **9**, 5652–5664.

31 A. Yang, B. Qiao, E. M. Strohm, J. Cao, Z. Wang, X. Yuan, Y. Luo and Y. Sun, Thrombin-responsive engineered nanoexcavator with full-thickness infiltration capability for

pharmaceutical-free deep venous thrombosis theranostics, *Biomater. Sci.*, 2020, **8**, 4545–4558.

32 Y. Yuan, S. Diao, D. Zhang, W. Yi, B. Qi, X. Hu, C. Xie, Q. Fan and A. Yu, A targeted activatable NIR-II nanoprobe for positive visualization of anastomotic thrombosis and sensitive identification of fresh fibrinolytic thrombus, *Mater. Today Bio*, 2023, **21**, 100697.

33 C. Quintana, M. P. Cifuentes and M. G. Humphrey, Transition metal complex/gold nanoparticle hybrid materials, *Chem. Soc. Rev.*, 2020, **49**, 2316–2341.

34 W. Tang, W. Fan, J. Lau, L. Deng, Z. Shen and X. Chen, Emerging blood-brain-barrier-crossing nanotechnology for brain cancer theranostics., *Chem. Soc. Rev.*, 2019, **48**, 2967–3014.

35 S. Kargozar, F. Baino, S. Hamzehlou, M. R. Hamblin and M. Mozafari, Nanotechnology for angiogenesis: opportunities and challenges, *Chem. Soc. Rev.*, 2020, **49**, 5008–5057.

36 J. A. De Pablo-Moreno, L. J. Serrano, L. Revuelta, M. J. Sánchez and A. Liras, The Vascular Endothelium and Coagulation: Homeostasis, Disease, and Treatment, with a Focus on the Von Willebrand Factor and Factors VIII and V, *Int. J. Mol. Sci.*, 2022, **23**, 8283.

37 W. Zhang, J. Wang, Z. Xie, H. Zou, Q. Chen, L. Xu, L. Hu, N. Fang, J. Xu, J. Zhou, J. Liu, H. Ran, Z. Wang, Y. Zhang and D. Guo, Antithrombotic Therapy by Regulating the ROS-Mediated Thrombosis Microenvironment and Specific Nonpharmaceutical Thrombolysis Using Prussian Blue Nanodroplets, *Small*, 2022, **18**, e2106252.